Rotation and magnetic field in the Be star ω Orionis

C. Neiner, A.-M. Hubert, Y. Frémat, M. Floquet, S. Jankov, O. Preuss, H.F. Henrichs, J. Zorec

A&A 409, 275–286 (2003)
DOI: 10.1051/0004-6361:20031086

Astronomy & Astrophysics

Rotation and magnetic field in the Be star ω Orionis[⋆,⋆⋆]

C. Neiner[1,2,3], A.-M. Hubert[1], Y. Frémat[1], M. Floquet[1], S. Jankov[4,5], O. Preuss[6], H. F. Henrichs[2], and J. Zorec[7]

[1] GEPI/UMR 8111 du CNRS, Observatoire de Paris-Meudon, France
[2] Sterrenkundig Instituut "Anton Pannekoek", Universiteit van Amsterdam, The Netherlands
[3] RSSD, ESTEC / ESA, Keplerlaan 1, 2201 AZ Noordwijk ZH, The Netherlands
[4] Département d'Astrophysique de l'Université de Nice-Sophia Antipolis, UMR 6525 du CNRS, France
[5] Astronomical Observatory Beograd, MNTRS 1940, Volgina 7, 11050 Beograd, Serbia
[6] Max Plank Institut für Aeronomie, Lindau, Germany
[7] Institut d'Astrophysique de Paris (IAP), France

Received 21 March 2003 / Accepted 7 July 2003

Abstract. ω Ori is a B2IIIe star for which rotational modulation and non-radial pulsations (NRP) have been recently investigated from two independent observational campaigns in 1998 and 1999. Putting the data of these 2 campaigns together, and adding data obtained in 2001, we search for multiperiodicity in the line profile variations and evidence for outbursts. From new spectropolarimetric data obtained at the Télescope Bernard Lyot (TBL, Pic du Midi, France) in 2001 we also measure the Stokes V parameter in the polarised light. We find evidence for the presence of a weak magnetic field in ω Ori sinusoidally varying with a period of 1.29 d. The equivalent widths (EW) of the wind sensitive UV resonance lines also show a variation with the same period, which we identify as the rotational period of the star. We propose an oblique rotator model and derive $B_{\rm pol}$ = 530 ± 230 G to explain the observations. Moreover, we carry out an abundance analysis and find the star to be N-enriched, a property which is shared with other magnetic stars. We propose ω Ori as the first known classical Be star hosting a magnetic field.

Key words. stars: magnetic fields – stars: oscillations – stars: winds, outflows – stars: individual: ω Ori

1. Introduction

ω Ori is a well-known rapidly rotating classical Be star with spectral type B2IIIe. This type of star exhibits strongly variable winds evidenced by rapidly variable UV resonance lines of highly ionised species, as well as spectral and photometric variations on timescales from hours to decades. The phases of emission in the optical and IR lines of hydrogen and several other species are called the Be phenomenon and most likely reflect changes in the structure of the circumstellar disk due to episodic ejections of mass. The flattened envelope is thought to be related to the usually high rotational velocities of Be stars. However, rotation by itself cannot explain the formation of the disk. Non-radial pulsations and magnetic fields have been proposed as possible additional mechanisms to explain the Be phenomenon (e.g. Osaki 1986; Underhill 1987).

Recently the role of rotational modulation and NRPs was investigated to explain short-term periodic variations detected in the Be star ω Ori, thanks to two international multisite campaigns carried out independently at the end of 1998 (Neiner et al. 2002, hereafter N02) and at the end of 1999 (Balona et al. 2001, hereafter B01).

B01 associated the period of about P = 0.97 d (f = 1.03 c d^{-1}) detected in the light and line-profile variations to the rotational period and argued that the periodic variation is due to clouds co-rotating with the star.

From their analysis of data provided by the MuSiCoS (MUltiSIte COntinuous Spectroscopy) 1998 campaign, N02 concluded that both NRPs and rotational modulation of orbiting clouds are needed to explain the multiperiodicity detected in ω Ori. The star and the inner layers of the circumstellar matter were found to pulsate non-radially with the period P_1 = 0.97 d (f_1 = 1.03 c d^{-1}) associated with a NRP mode with l = 2 or 3 and $|m|$ = 2. Another period P_2 = 2.17 d (f_2 = 0.46 c d^{-1}) was also detected and attributed to material temporarily orbiting around the star then diluting in the circumstellar environment. The occurrence of

Send offprint requests to: C. Neiner,
e-mail: cneiner@rssd.esa.int

⋆ Based on observations obtained using the Musicos spectropolarimeter at the Observatoire du Pic du Midi (France), during the MuSiCoS 98 campaign (Neiner et al. 2002), and by Balona et al. (2001). Based on INES data from the International Ultraviolet Explorer (IUE) satellite.

⋆⋆ Table 7 is only available in electronic form at the CDS via anonymous ftp to cdsarc.u-strasbg.fr (130.79.128.5) or via http://cdsweb.u-strasbg.fr/cgi-bin/qcat?J/A+A/409/275

an emission line outburst was deduced from the behavior of spectral parameters. Analogy with outbursts detected in μ Cen by Rivinius et al. (1998a) was found. At least one other period of about $P_3 = 1.22$ d ($f_3 = 0.82$ c d^{-1}) with a weak signal power was seen in the stronger He I lines, compatible with the one detected in UV data of February 1996 (Peters 1996) and close to the rotational period that N02 derived from their analysis of fundamental stellar parameters.

The present paper reports on a global analysis of data collected during both multisite spectroscopic campaigns mentioned above. The ones obtained in 1999 were kindly put at our disposal by C. Aerts and L. A. Balona. New data acquired at the end of 2001 at TBL (Pic du Midi, France) were added.

The aim of this study is to:
(i) search for multiperiodicity in all data put together and collected over a 4-year span, in particular to search for frequencies close to the powerful frequency $f_1 = 1.03$ c d^{-1} detected separately by B01 and N02, to investigate a possible beating effect of NRPs, similar to the one reported by Rivinius et al. (1998b) in the case of μ Cen;
(ii) search for evidence for a possible outburst in 1999 and 2001 data;
(iii) study the behavior of spectral quantities expected to vary with the proposed rotational frequency around $f_3 = 0.82$ c d^{-1};
(iv) obtain measurements of the Zeeman signature in the Stokes V parameter from the spectropolarimetric data obtained in 2001 at TBL, to determine whether the star hosts a magnetic field.

In Sect. 2 we present the observations. The spectral variations are studied in Sect. 3, in the frame of non-radial pulsations and rotational modulation. Section 4 focuses on the variations in the emission components of emission lines. We reconsider the $v \sin i$ value of the star in Sect. 5 and determine its stellar parameters and the chemical abundances. In Sect. 6 we re-analyse the IUE data of ω Ori to derive the rotation period. In Sect. 7 we report on the possible discovery of a magnetic field in ω Ori and propose an oblique magnetic rotator model. The results are discussed and conclusions are summarised in Sect. 8.

2. Observations

2.1. Spectroscopy

Spectra were obtained during the MuSiCoS campaign from November 23 to December 15 in 1998. This campaign used 8 telescopes around the world simultaneously to obtain continuous spectroscopy. 249 spectra of ω Ori were collected over the 22 night run, well distributed in time thanks to the multisite observations. The data are described in detail in N02.

Spectra were also obtained from November 17 to December 7 in 1999. The data are described in B01. In the present study we only use the 296 spectra obtained at SAAO with the GIRAFFE spectrograph and the 303 spectra obtained at ESO La Silla with the Coralie spectrograph, as they are of better quality.

Finally, spectropolarimetric data were obtained at TBL (Pic du Midi, France) from December 19 to 24 in 2001 with the spectropolarimeter Musicos (see next subsection). The star was observed during 8.5 hours per night. The individual subexposures of Stokes V measurements, i.e. 152 spectra, were used for spectroscopic study.

Table 1. Journal of TBL observations of ω Ori obtained in December 2001. Column 1 indicates the number of the polarimetric sets. Columns 2 and 3 show the day and time of the beginning of observations. Column 4 indicates how many polarimetric sets or individual subexposures were obtained.

#	Day	Start UT h:min	Sets/ Individual
1–8	19	19:23	7 sets
9–16	20	19:29	7 sets
17–24	21	19:14	7 sets
25–30	22	19:25	6 sets + 4 ind
31–36	23	19:46	5 sets + 8 ind

The three sets of spectra were obtained close to a minimum of emission in the long-term Be period observed by the French association of amateurs AUDE early 2000 (Buil 2001).

2.2. Spectropolarimetry

The Musicos échelle spectropolarimeter, with a resolving power $R = 35\,000$, is mounted at the Cassegrain focus of the 2 m Télescope Bernard Lyot (TBL) at Pic du Midi in France. Stellar light is collected in a 2″ entrance aperture in the spectral range 4500–6600 Å. Linear/circular sheet polarisers can be inserted in the beam. One half-wave and one quarter-wave retarder can also be inserted and rotated to achieve a linear or circular analysis of the stellar light.

To detect stellar magnetic fields, one analyses the circular polarisation of the light. The observing strategy is to set the quarter-wave plate and take 4 subexposures: one at azimuth $-45°$, two at azimuth $45°$, and one more at azimuth $-45°$. This gives a complete Stokes V measurement. 36 Stokes V measurements were obtained in December 2001 (see Table 1).

A dedicated software package, ESpRIT (Donati et al. 1997), is available at TBL to reduce and analyse the data. We implemented an improved version of ESpRIT, using two series of flat-fields taken in the two positions of the quarter-wave plate, which optimizes the extraction of the échelle orders. Fringes were removed using a fringe template extracted from the Stokes V spectrum of a non-magnetic star (γ Peg) obtained during the first night of the run and reduced in the same way as ω Ori.

After applying the Least-Squares Deconvolution (LSD), a cross-correlation technique developed by Donati et al. (1997), one can detect a stellar magnetic field through the Zeeman signatures generated in the shape and polarisation state of spectral line profiles. The LSD method combines the very small circularly polarised signatures, properly weighted, of all available line profiles in the spectrum to increase the signal to noise ratio. For ω Ori, only 80 spectral lines, without emission, could

Table 2. Journal of IUE observations of ω Ori obtained in February 1996. Column 1 indicates the number of the spectrum in the IUE archives. Column 2 gives the exposure time. The Heliocentric Julian Date (HJD) minus 2 450 000 at mid-exposure is given in Col. 3.

Image	Exp	Mid	Image	Exp	Mid	Image	Exp	Mid
SWP	s	HJD	SWP	s	HJD	SWP	s	HJD
56677	139.5	115.75	56706	69.5	117.14	56734	69.5	118.09
56680	84.7	116.11	56707	69.5	117.16	56735	69.5	118.12
56681	84.7	116.14	56708	69.5	117.18	56736	69.5	118.14
56682	84.7	116.16	56709	69.5	117.21	56737	69.5	118.18
56683	84.7	116.19	56710	69.5	117.24	56738	69.5	118.21
56684	84.7	116.22	56711	69.5	117.26	56739	69.5	118.25
56685	84.7	116.33	56712	69.5	117.29	56740	69.5	118.30
56686	84.7	116.36	56713	69.5	117.31	56741	69.5	118.32
56687	84.7	116.39	56714	69.5	117.34	56742	69.5	118.35
56688	84.7	116.41	56715	69.5	117.37	56743	69.5	118.37
56689	69.5	116.44	56716	69.5	117.39	56744	69.5	118.51
56690	69.5	116.46	56717	69.5	117.41	56745	69.5	118.54
56691	69.5	116.48	56718	69.5	117.43	56746	69.5	118.56
56692	69.5	116.50	56719	69.5	117.45	56747	69.5	118.58
56693	69.5	116.53	56720	69.5	117.58	56748	69.5	118.60
56694	69.5	116.55	56721	69.5	117.60	56749	69.5	118.63
56695	69.5	116.58	56722	69.5	117.63	56750	69.5	118.65
56696	69.5	116.60	56723	69.5	117.65	56751	69.5	118.67
56697	69.5	116.62	56724	69.5	117.67	56752	69.5	118.70
56698	69.5	116.65	56725	69.5	117.69	56753	69.5	118.72
56699	119.5	116.77	56726	69.5	117.72	56754	69.5	118.74
56700	69.5	116.79	56727	69.5	117.74	56755	69.5	118.76
56701	69.5	116.82	56728	69.5	117.78	56756	69.5	118.79
56702	69.5	116.85	56729	69.5	117.81	56757	69.5	118.82
56704	69.5	117.09	56730	69.5	117.84	56758	69.5	118.84
56705	69.5	117.11	56733	69.5	118.07			

be used to provide a mean Stokes V profile. These photospheric lines correspond to ions of He I, C II, C III, N II, O II, Ne I, Al III, Si II, Si III, S II, Fe III, with line depths from 0.02 to 0.46 and Landé factors from 0.67 to 2.01. The line depths and Landé factors are extracted from Kurucz models provided in the ESpRIT package (see Donati et al. 1997). The method assumes that the intrinsic broadening is similar for all lines.

2.3. Ultraviolet spectroscopy

Many high-dispersion ultraviolet spectra ($R \simeq 18\,000$) of ω Ori were obtained with the Short Wavelength Prime (SWP) camera onboard the IUE satellite during more than 15 years. Table 2 presents the journal of the 77 spectra of ω Ori obtained during a campaign with nearly continous coverage over three days in February 1996 (Peters 1996), which were retrieved from the INES database (`http://ines.laeff.esa.es/`). The other available spectra are much less homogeneously distributed over the years and not taken during a Balmer emission phase. The structure of their UV wind profiles appears to be different and therefore only the February 1996 data were considered in this work. Image SWP 56716 has unusual noise characteristics and was ignored. Thus, we used the remaining 76 spectra to ensure the highest homogeneity. The spectra were mapped on a uniform wavelength grid of 0.1 Å, which effectively degraded the resolving power to 12 000−15 000. The signal-to-noise ratio of the spectra is at best about 24.

Table 3. Frequencies detected in the three sets of data for each studied line. The He I 6678 and Mg II 4481 lines are outside the wavelength range of the Musicos spectrograph, and therefore not studied in 2001.

		Frequency (c d^{-1})					
Line	Year		$f_{\rm rot}$	2-f_1	f_1		2f_1
He I 4713	1998	0.48	0.82		1.01		2.02
	1999	0.50	0.75	0.92		1.06	
	2001	0.52	0.81	0.94	1.03		2.02
He I 4921	1998	0.47	0.75	0.89	1.03		2.03
	1999	0.51		0.89?		1.07	2.06
	2001	0.51	0.73	0.93		1.06	2.06
He I 5876	1998	0.48	0.75	0.97	1.03	1.07	2.02
	1999	0.50			1.03	1.07	2.06
	2001	0.51	0.82		1.00	1.09	2.03
He I 6678	1998	0.46	0.82	0.93	1.03		2.09
	1999	0.50			1.03	1.07	2.06
Mg II 4481	1998	0.48	0.76	0.93	1.04		2.05
	1999	0.50	0.75	0.94?	1.03	1.07	2.06
Si III 4553	1998	0.48	0.80	0.92	1.04		2.07
	1999		0.85		1.03	1.05	2.06
	2001	0.47	0.8	0.96		1.07	2.04

3. Spectral variations

3.1. Time series analysis of line profile variations

We re-analysed the line profile variations (lpv) of the main lines for each campaign from 1998, 1999 and 2001 individually and for the three campaigns put together. Results are shown in Table 3 which gives the main detected frequencies for each line.

First the three sets of data are analysed separately with the same methods as in N02: the Restricted Local Cleanest (RLC) and Least Square (LS) methods. In each set the first frequency $f_1 = 1.03$ c d^{-1} is always detected, with generally its first harmonic 2.06 c d^{-1}. A second frequency 1.07 c d^{-1}, close to the first one, is often detected. Nevertheless the phase velocity associated to this frequency is inaccurate due to the weakness of the power of the signal and to the lack of homogeneity of spectra obtained with various instrumentation during the three runs.

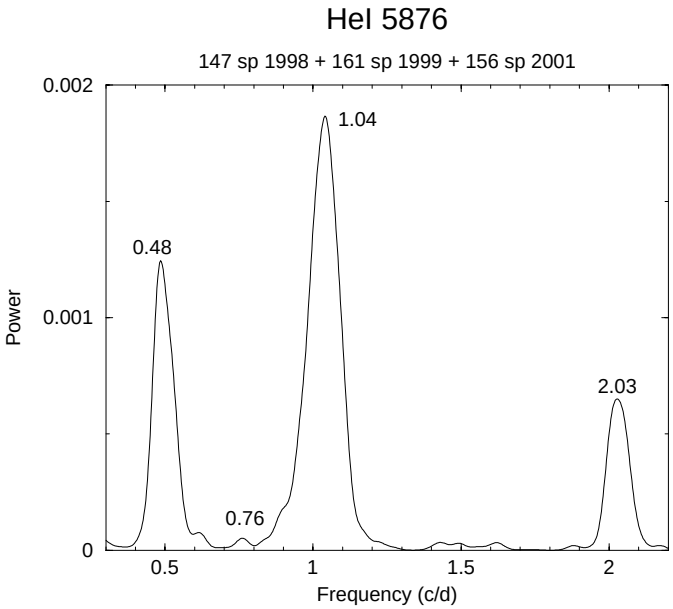

Fig. 1. Example of power spectrum obtained for the He I 5876 line with the three datasets.

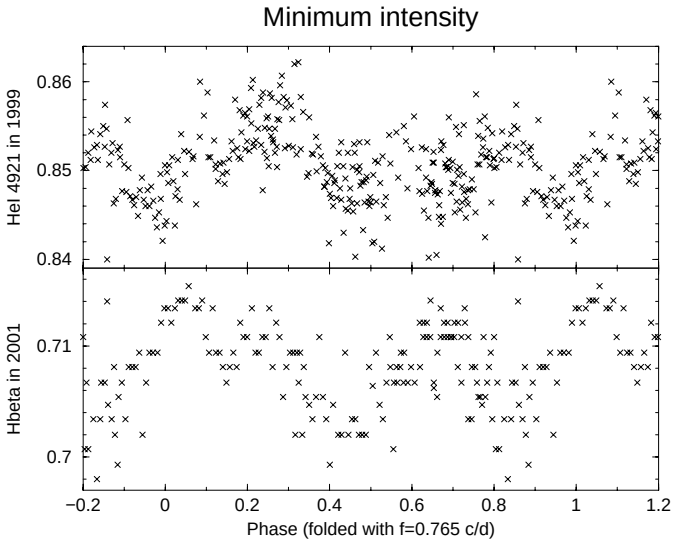

Fig. 2. Variations of the minimum intensity of the He I 4921 line observed in 1999 and the Hβ line observed in 2001, folded in phase with $f = 0.765$ c d^{-1} and with HJD$_0$ = 2 451 499.0 and 2 452 262.6 respectively.

The frequency around 0.8 c d^{-1} is sometimes present in periodograms of each of the three campaigns but it always has a very weak signal power. It is associated with the rotation period of the star proposed in N02. Marginal frequencies are also detected at 0.51 (in 1999 and 2001), 0.56 (in 1998), 0.93 (2-day alias of 1.07 c d^{-1}, in 2001) and 1.17 c d^{-1} (2-day alias of the rotation frequency, in 1999).

The analysis of the three sets of data put together shows similar results. For this investigation only one spectrum out of four was used for the SAAO and ESO data obtained in 1999, in order to avoid giving a higher weight to this campaign. An example of the power spectrum obtained for the He I line 5876 is shown in Fig. 1. Note that the frequency resolution corresponds to the one from individual observing runs, rather than to the resolution expected from the complete data set (1998–2001), because the deconvolution algorithm cannot get rid of complex aliasing problem due to the large gaps between successive observing runs.

We obtained a coherent phase distribution only for the signal associated with the frequency 1.03 c d^{-1}. The data used in this study were taken with various instrumentation and a rather moderate signal to noise ratio (∼150). The search for other frequencies with low power close to the frequency at 1.03 c d^{-1} is thus difficult. We conclude that there is one main frequency of non-radial pulsations at 1.03 c d^{-1}. If other pulsation frequencies exist, high quality homogeneous data such as satellite data will be necessary to confirm them.

3.2. Minimum intensity

The minimum intensity variation (i.e. the variation of the central depth) is investigated for lines with the best signal to noise ratio in 1999 and 2001. We do not search in the data taken in 1998, as the number of observations per line for each site is too low to expect to detect such variations.

In Fig. 2 variations of the minimum intensity of the He I 4921 line observed in 1999 at ESO (Coralie data) and of the Hβ line observed in 2001 with the best S/N ratio, are folded in phase with $f = 0.765$ c d^{-1}. Because the frequency is not precise enough, the phases of 1999 and 2001 are not correlated. However, it seems for both years that the minimum intensity varies with this period $P \sim 1.3$ d associated with the rotation, showing a double-wave, i.e. two maxima and minima in one period.

4. Emission lines

At the time of MuSiCoS 1998 observations, emission was still present in the wings of some lines during the campaign (e.g. Hα, Hβ, He I 5876, 6678 and 7065, Si II 6347, C II 6578 and 6583). The Hα line had a double-peaked emission ($R \sim V$) profile with $I_{\rm max}/I_{\rm c} = 1.4$. At the end of 1999 the emission was fainter, $I_{\rm max}/I_{\rm c} \sim 1.15$ for Hα; emission was still present in the red helium lines but very weak in the He I 5876 line and sometimes absent in the He I 6678 line. The Si II 6347 and C II 6578 and 6583 lines were purely photospheric. In 2001 the emission was again increasing with $I_{\rm max}/I_{\rm c} = 1.3$ at Hα.

4.1. V and R peak intensities

Figure 3 shows the violet (V) and red (R) intensities of the He I 5876 line during the three observation campaigns. In 1998 the V and R peak intensities of red He I lines fluctuated in a regular fashion with a gradual increase over about 12 days from the middle of the run (start of an outburst). In 1999 the V and R peaks of He I 5876 also fluctuated in intensity and more clearly between HJD 2 451 509 and 2 451 514 when the temporal coverage is better, since both sites were operating at that time. In 2001 the V and R peak intensities of the He I 5876 and Hβ lines were globally increasing over the 5 day

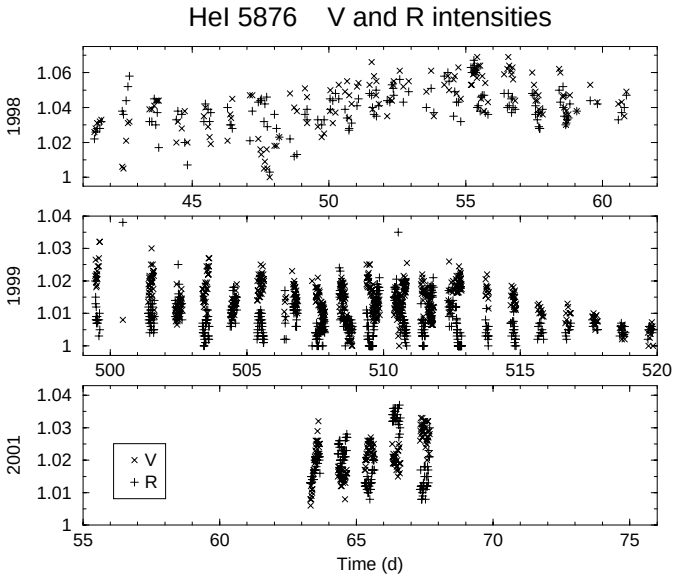

Fig. 3. Variations of the intensity of the V and R components of the He I 5876 line during the three observing runs. The data obtained in 2001 (in HJD minus 2 452 200) are plotted on the same time scale as the data obtained in 1998 (in HJD minus 2 451 100) and 1999 (in HJD minus 2 451 000) to make the comparison easier.

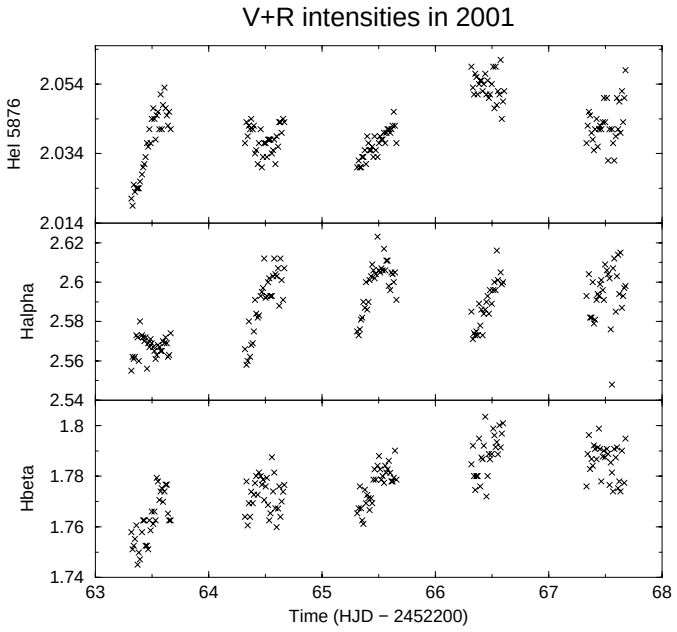

Fig. 4. Variations of the intensity of the V plus R components of the He I 5876, Hα and Hβ lines during the observations taken in 2001.

run (Fig. 4). A rapid variation is also observed, which seems to correspond to the rotation period.

4.2. Separation between V and R peaks

The peak separation between the V and R components of the red He I lines was found to be increasing during the MuSiCoS 1998 campaign (see N02). Associated with an increase of the $V + R$ quantity, this indicates the occurrence of an outburst. No similar trend could be derived from data

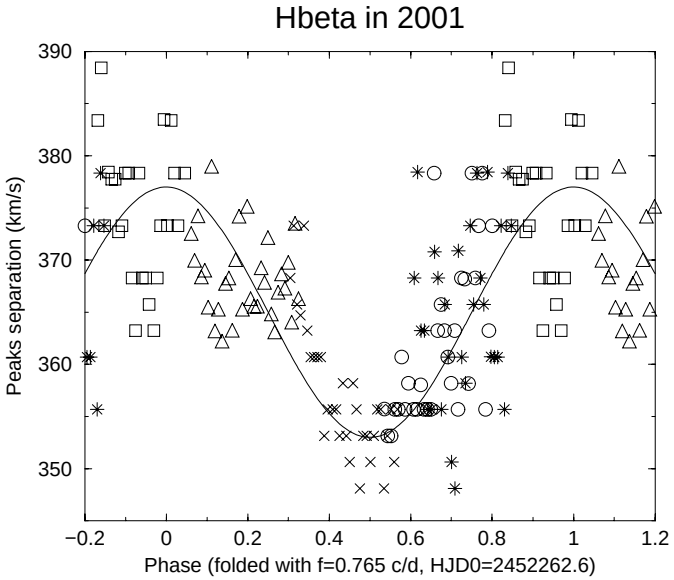

Fig. 5. Variations of the separation between the V and R peaks in the Hβ line observed in 2001. Each of the five nights of observations is represented by a different symbol.

obtained in 1999. In 2001 we find again a very weak tendency of an increase of the peak separation in Hβ, associated with an increase of $V + R$ quantity (this latter was also seen in He I 5876), which suggests that the beginning of an outburst was probably observed at that time. The peak separation of the Hβ line observed in 2001 also varies as a single wave in phase with the frequency 0.765 c.d^{-1} associated with the rotation period (Fig. 5).

4.3. V over R ratio

The V/R ratio in the He I 5876 and 6678 lines were modulated by the frequency 1.03 c d^{-1} in 1998 but also by the frequency 0.46 c d^{-1} mainly in the first part of the run. This latter frequency was attributed by N02 to a cloud temporarily rotating around the star.

In 1999, the emission was fainter in the red He I lines. Therefore the V, R and V/R variations were more difficult to analyse. Sometimes the emission completely disappeared in the V or R component of the He I 6678 line (as in the ESO spectrum at HJD 2 451 508.7). Moreover the location of the V emission component of the He I 6678 line in the ESO spectra at the beginning of an échelle order made the determination of the continuum in this region uncertain. The V/R ratio of the He I 5876 line was weakly modulated with the frequency 1.11 c d^{-1} and dominated by the frequency 1.53 c d^{-1} (or twice 0.765 c d^{-1}), mainly between HJD 2 451 509 and 2 451 514; the V/R ratio of the He I 6678 line was also dominated by the 1.53 or twice 0.765 c d^{-1} frequency (Fig. 6, upper and middle panels). This latter frequency can be related to the rotational frequency as determined in N02, which suggests the presence of two corotating regions around the star such as the clouds proposed by B01 to explain lpvs.

In 2001 the V/R ratio of He I 5876 was slightly increasing in amplitude over the 5-day run. It seemed again to be

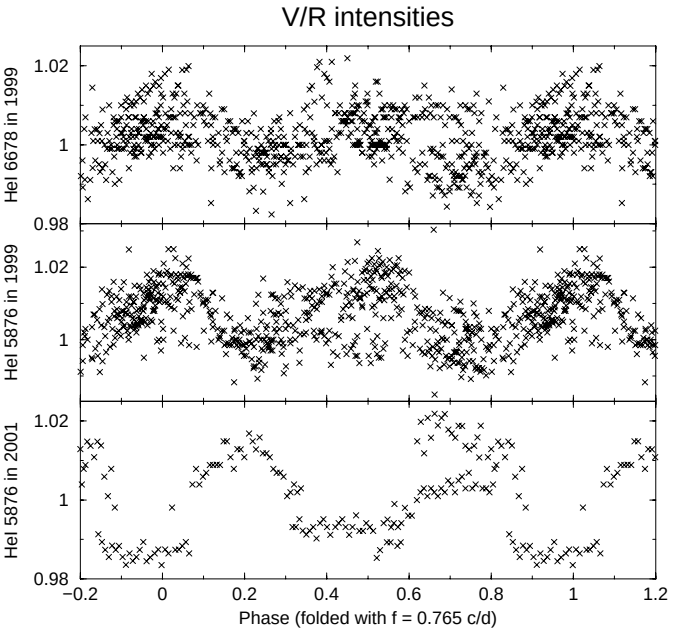

Fig. 6. Variations of the intensity of the V/R components of the He I 6678 line observed in 1999 and of the He I 5876 line during the observations taken in 1999 and 2001. The plots are folded in phase with $f = 0.765$ c d^{-1} and with HJD$_0$ = 2 451 499 and 2 452 262.6 respectively.

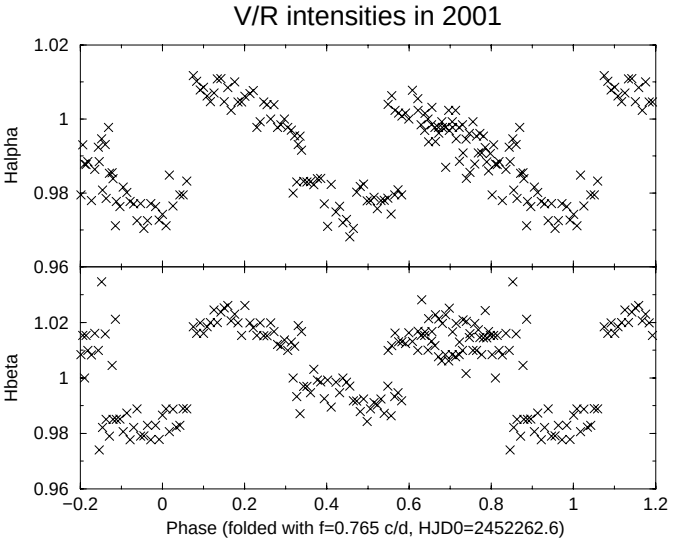

Fig. 7. Variations of the intensity of the V/R components of the Hα and Hβ lines observed in 2001. The plots are folded in phase with $f = 0.765$ c d^{-1} and HJD$_0$ = 2 452 262.6.

modulated by the frequency 0.765 c d^{-1} or its double, related to the rotation period (Fig. 6, lower panel).

The V/R ratio in Hα and Hβ show clear variations with the rotation period or its half. It slowly decreases from phase 0.1 to 0.6, then suddenly increases, slowly decreases again from phase 0.6 to 1.1 and then suddenly increases again (Fig. 7). This behavior can be associated with two corotating regions passing in front of the visible hemisphere of the star from the blue to the red edge, one after the other.

Table 4. Determined values of $v \sin i$ (km s^{-1}) for the C II 4267, Mg II 4481 and Si III lines obtained in 1999 using the Fourier transform analysis, compared to the values given by B01 for the same data and by N02 for the data obtained in 1998.

	$v \sin i$		
	N02	B01	this paper
Data obtained in	1998	1999	1999
C II 4267	178	214	169
Mg II 4481	185	233	180
Si III 4553	179	223	165

The frequency 1.03 c d^{-1} never dominated the modulation of the V/R ratio of red He I lines. The frequency 0.765 c d^{-1} is present at times during several consecutive days, which suggests that it is related with the motion of corotating regions such as clouds. Unfortunately the sample obtained in 2001 was too short for a detailed study and, in 1999, data were obtained at best during 12 hours per day, which is insufficient to follow the rotation of such clouds and induces strong aliases in periodograms.

5. Stellar parameters

5.1. v sin i

In N02, $v \sin i$ was determined for He I and metal lines with two methods. For all the lines, with both methods, the same value $v \sin i = 179 \pm 4$ km s^{-1} was found. In contrast, B01 found a similar value for the He I lines from spectral modeling but a higher value for the metal lines.

We investigate here the $v \sin i$ value of the data used in B01 with the Fourier analysis method used in N02. Details of this method can be found in N02. Results are shown in Table 4. We obtained a value of $v \sin i$ similar to what was found before for He I lines obtained in 1998 by N02.

5.2. Stellar parameters

We determine the fundamental parameters of ω Ori by fitting spectral line profiles obtained by averaging the Coralie spectra (B01).

As ω Ori is a Be star, the rotation is expected to affect its spectrum. In their recent paper, Chauville et al. (2001) showed that most of the Be stars rotate at the same angular velocity ratio $\omega = 0.795$ ($\omega = \Omega/\Omega_c$, where Ω_c is the critical angular velocity). At this level of rotation rates, the stars are generally supposed to flatten and to show non uniform temperature and density distributions at their surface. In practice, it means that a Be star may appear cooler and more evolved than it really is when one does not take into account these gravitational darkening effects.

To study the photospheric spectra of ω Ori, we therefore use the FASTROT computer code (Frémat et al. 2002; Frémat & Zorec 2003) based on an approach very similar to the one described by Collins et al. (1991, and references therein).

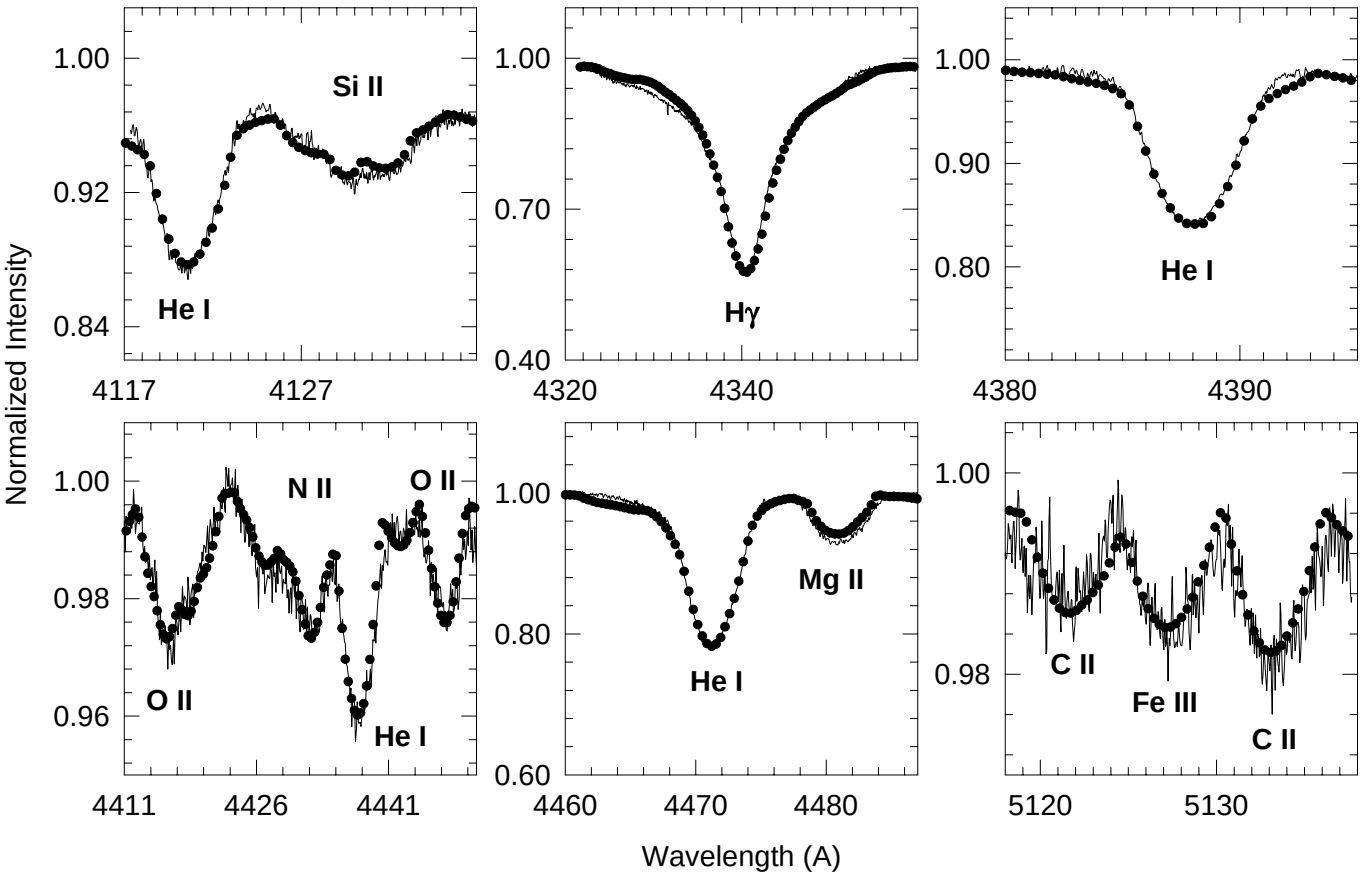

Fig. 8. Theoretical spectra (dots) compared to observations (solid line) from the Coralie spectrograph in the fitted spectral regions.

This code assumes a gravitational darkening law defined by the von Zeipel theorem and provides rotationally deformed line profiles.

NLTE plane-parallel atmosphere models represent the *local* temperature and density distributions at about 10 000 selected points on the stellar surface. These models are obtained with the TLUSTY198 and SYNSPEC45 computer codes (Hubeny & Lanz 1995). Microturbulence is assumed equal to 2 km s^{-1}, which is the average value proposed by Andrievsky et al. (1999) for NLTE computations of B-type stars.

Except for neutral oxygen which is treated with the MODION IDL package, the atomic models we use are those proposed by Hubeny & Lanz on TLUSTY's web site: H: 16 levels, He I: 24 levels, He II: 20 levels, C I: 8 levels, C II: 34 levels + 5 superlevels, C III: 12 levels, N I: 13 levels, N II: 35 levels + 14 superlevels, N III: 11 levels, O I: 14 levels + 8 superlevels, O II: 36 levels + 14 superlevels, O III: 9 levels, Si I: 6 levels, Si II: 36 levels + 4 superlevels, Si III: 12 levels.

The oscillator strengths adopted to study the carbon, nitrogen, oxygen and silicon transitions are from the NIST database and are added to the Kurucz line lists provided with SYNSPEC. Stark widths of the Si II and Si III spectral lines are derived from the results of González et al. (2000), Dimitrijevic et al. (2002) and Lanz et al. (1988).

Fundamental parameters of ω Ori are determined by fitting the observed He I 4388 and 4471 transitions together with the wings of Hγ. We use a least-squares method combined to a minimization procedure based on the MINUIT package developed at CERN. The code gives the possibility to adjust four parameters: the effective temperature $T_{\rm eff}^{\circ}$ and the gravity $\log g^{\circ}$ of the non rotating counterpart of the star, its angular velocity Ω, and its projected rotation velocity $v \sin i$. At each iteration, the stellar masses and radii are deduced by numerical interpolation on $T_{\rm eff}^{\circ}$ and $\log g^{\circ}$ in the evolutionary tracks computed by Schaller et al. (1992), assuming a solar metallicity. The critical angular velocity and the inclination angle i of the star are then derived.

The error bars on the fundamental parameters are estimated by assuming different sets of initial values during the fitting procedure. For example, the angular velocity ω is set at different values between its extreme limits 0.57 (for which $i = 90°$) and 0.99 (after which the star breaks). All the fits converge to $\omega = 0.81 \pm 0.1$, which is very similar to the average value found by Chauville et al. (2001). In the same way, the error bars on the effective temperature, superficial gravity and projected rotation velocity correspond to the largest deviation observed in all the fits.

The fit of the hydrogen and helium lines provides a good agreement with the values derived from the study of the TD1 UV fluxes, i.e. $T_{\rm eff} = 19\,500$ K. TD1 observations are corrected for interstellar reddening assuming a colour excess $E(B-V) = 0.13$ estimated by Fabregat & Reglero (1990) and using the extinction laws given by Cardelli et al. (1989) and O'Donnell (1994). A good agreement is also found with

Table 5. Stellar parameters of ω Ori obtained by fitting hydrogen and helium lines.

$T_{\rm eff}^{\circ}$	20 020 ± 700 K
$\log g^{\circ}$	3.53 ± 0.07
i	42 ± 7°
$v \sin i$	172 ± 11 km s^{-1}

Table 6. Chemical composition of ω Ori compared to the mean chemical composition of B stars, as derived by Gies & Lambert (1992) and of local B stars, as derived by Gummersbach et al. (1998). The logarithmic abundances $\log(\epsilon_N/\epsilon_\odot)$ are given relatively to the solar values compiled by Grevesse & Sauval (1998).

Ion	ω Ori	Gies & Lambert	Gummersbach
C II	0.00 ± 0.07	−0.32 ± 0.16	−0.32 ± 0.15
N II	0.26 ± 0.10	−0.11 ± 0.22	−0.20 ± 0.12
O II	−0.09 ± 0.06	−0.15 ± 0.14	−0.27 ± 0.09

the computation of the Si II 4131 and Si III 4553 spectral lines, i.e. $T_{\rm eff}$ = 20 600 K and $\log g$ = 3.43. Those test fits assume the inclination angle and the projected rotational velocity fixed at the values given in Table 5.

The fitting procedure is then applied assuming several values of the helium abundance. The best agreement between observations and models is obtained for a solar value of the He/H ratio with an accuracy equivalent to the adopted helium abundance step: He/H = 0.10 ± 0.01.

The same approach is used to estimate the CNO chemical composition of ω Ori (Fig. 8). In Table 6, the logarithmic abundances are given relatively to the solar values compiled by Grevesse & Sauval (1998). Species other than carbon, nitrogen or oxygen were taken at their solar values. C, N, O are usually found to be underabundant in B stars, compared to the solar values (Gies & Lambert 1992; Gummersbach et al. 1998). This is not found in ω Ori, for which C and O have the same abundances as in the Sun and N is found to be enriched.

6. UV stellar wind

It is well known that the wind-sensitive doublet resonance lines of C IV 1550 and Si IV 1400 are variable in this star (e.g. Sonneborn et al. 1988). From a 3-day IUE campaign, Peters (1996) found that the C IV doublet varies with a period of about 1.21 d.

The top panels of Fig. 9 show an overplot of the IUE C IV and Si IV profiles, respectively, along with their variability signatures in the bottom panels. The variability occurs mainly in the strength of the line over a given range in velocity space, extending from −1000 to +600 km s^{-1} for the whole doublet. The expected variability is obtained using a noise model for such IUE spectra as derived by Henrichs et al. (1994) with parameters A = 24.1 and $B = 7.1 \times 10^{-10}$.

We measure the equivalent width (EW) of the C IV and Si IV lines between −600 and −100 km s^{-1} with the continuum chosen at 4×10^{-10} erg cm^{-2} s^{-1} Å^{-1} and

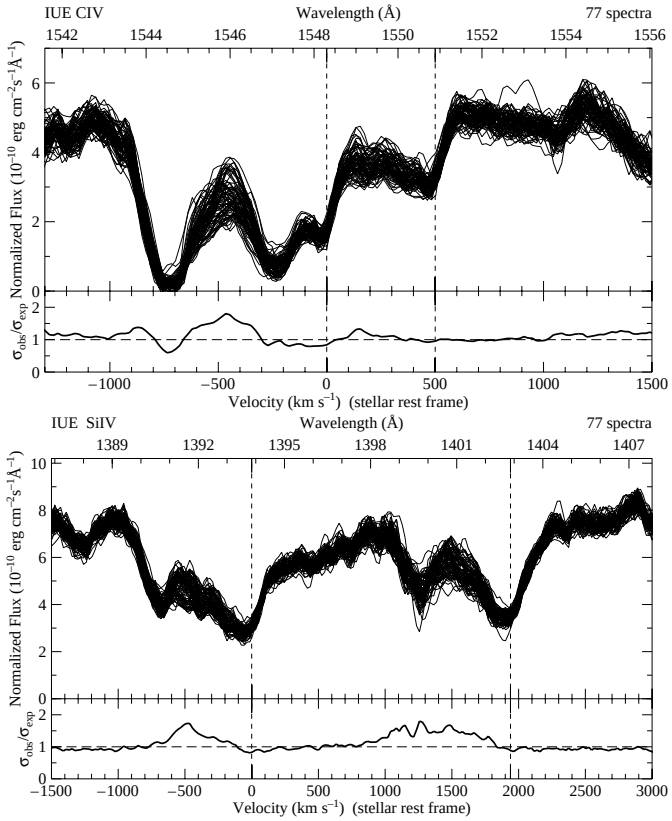

Fig. 9. Top panels: variation in the wind profiles of the UV C IV and Si IV lines; the fluxes are normalised to the mean spectrum. Bottom panels: variability signature, measuring the ratio of the observed variance (due to variability) to the expected variance (due to noise).

6×10^{-10} erg cm^{-2} s^{-1} Å^{-1} respectively and compute a least-squares fit of a sinusoid. Weights are assigned relative to the error bars of each datapoint. The result of the fit of the function

$$f(t) = a + b \sin\left(2\pi\left(\frac{t}{P} + \phi\right)\right) \quad (1)$$

for the C IV doublet gives a reduced χ^2 = 0.14, with parameters: a = 1.39 ± 0.01 Å, b = 1.74 ± 0.01 Å, ϕ = 0.27 ± 0.24 and a period P = 1.286 ± 0.023 d. The minima occur at HJD = 2 450 117.08 ± 0.62 + (1.286 ± 0.029) × N.

The period is identified with the rotation period of the star. The equivalent width of the C IV line as a function of rotational phase is plotted in Fig. 10, with the best fit overplotted. The equivalent width of the Si IV line is also shown.

7. Magnetic field

7.1. Measurements

Due to the small amount of available lines and to the high rotation velocity of the star, the magnetic measurements have large error bars. Table 7 (available at CDS) shows the longitudinal magnetic field value B, its error bar σB, the null polarisation N, which gives an indication of the pollution by non-stellar effects and should be zero for a perfect measurement, and its error σN.

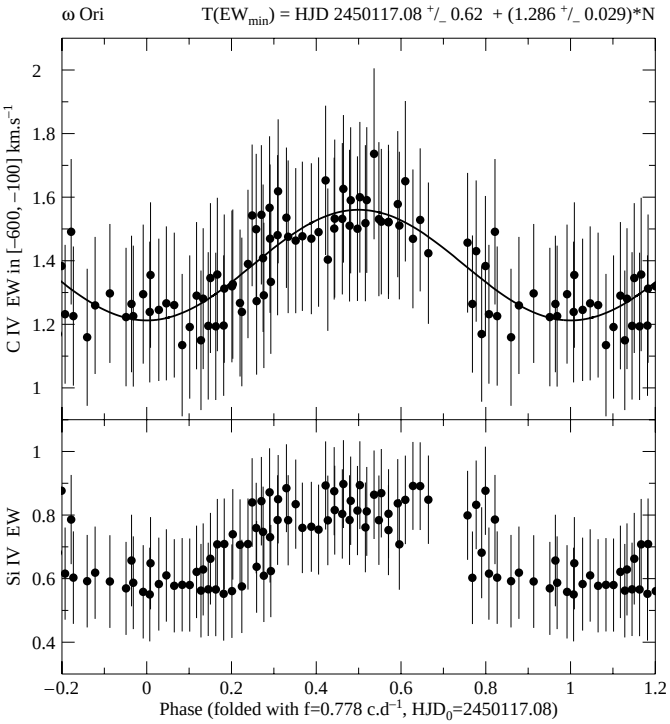

Fig. 10. Equivalent width variations (in Å) of the UV C IV and Si IV lines, folded in phase with the rotational period $P = 1.286$ d. The best fit is overplotted.

The exposure time for each subexposure was 15 min, i.e. about 1/100 of the pulsation period, to avoid smearing of the magnetic signal because of the pulsations. Although no strong signature appears in the individual Stokes V profiles, the measured value of the longitudinal component of the magnetic field is found to vary in phase with the UV period. A sinusoidal fit through the magnetic data gives an amplitude of the longitudinal component of $B_l = 80 \pm 40$ G around the average value of $B_0 = 74 \pm 28$ G, and a period of 1.29 ± 0.11 d, with $\chi^2 = 0.11$. This fit is shown as a solid line in Fig. 11. The period is, within the error bar, identical to the UV period derived in Sect. 6. We consider this coherent variation of the magnetic measurements in phase as an evidence for the presence of a weak longitudinal magnetic field in ω Ori. From the derived phase we determine that the maximum field occurs at HJD $2\,452\,265.19 \pm 0.38 + N \times 1.29 \pm 0.11$.

In the frame of the oblique magnetic rotator model (see Shore 1987) this period of variation corresponds to the rotation period of the star. The obtained period, corresponding to a frequency of $f = 0.775$ c d^{-1}, is consistent with the value $f = 0.73$ c d^{-1} obtained in N02, $f = 0.77$ c d^{-1} obtained from the V/R analysis (Sect. 3.4.3) and $f = 0.78$ c d^{-1} obtained from the UV stellar wind analysis (Sect. 6). Due to the uncertainties we could not uniquely relate the UV phase with the magnetic phase.

7.2. Oblique magnetic rotator model

We have found a weak varying longitudinal field in ω Ori, consistent with an oblique magnetic dipole with a rotational period of 1.29 d.

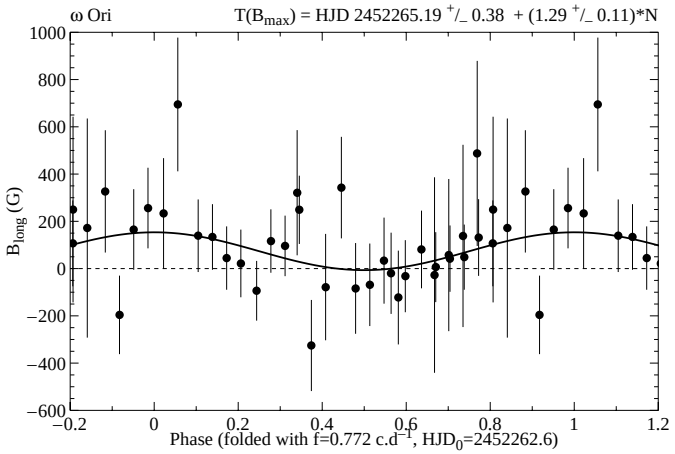

Fig. 11. Variations of the longitudinal component of the magnetic field, folded in phase with the period $P = 1.29$ d.

For a dipolar field, the ratio of the magnetic extremes $r = B_{\max}/B_{\min}$ is related to the inclination angle i and the angle β between the magnetic and the rotation axis via (see Shore 1987)

$$r = \frac{\cos(i-\beta)}{\cos(i+\beta)}. \quad (2)$$

In the case of ω Ori we find $r = -26$ with a large range depending on the error bars $-26 \leq r \leq 14$. If we adopt an inclination angle $i = 42^{49}_{35}{}^\circ$ as obtained in Sect. 4.2, we obtain $\beta = 50^{78}_{17}{}^\circ$.

With these values, $i + \beta = 92^{113}_{66}{}^\circ$, which is close to 90° and therefore one of the two magnetic poles is situated just at the edge of the visible hemisphere.

With this configuration it is expected that the variation in the UV lines sensitive to the wind shows only one maximum per period (Shore & Brown 1990), as indeed seen in Sect. 6 (Fig. 10).

With the known angles i and β, mean longitudinal field B_0 and amplitude of variations of the longitudinal component B_l, the strength of the magnetic field at the poles, i.e. the maximum field, can be determined by using a centered oblique dipolar model. The model we used is described in Neiner et al. (2003b). We used a limb darkening coefficient $k = 0.4$ as established by Claret (2000) for this kind of star. We obtained $B_{\rm pol} = 530^{760}_{300}$ G. A greyscale plot of the magnetic field in the visible hemisphere is shown in Fig. 12.

8. Discussion and conclusion

8.1. Pulsations

We confirm that the frequency $f_1 = 1.03$ c d^{-1}, already detected by N02 in the 1998 data and B01 in the 1999 data, is also found in the data obtained in 2001. We associate this frequency with a non-radial pulsation mode (see N02).

A second frequency at about $f = 0.77$ c d^{-1} is detected and associated with the rotation period (see Sect. 8.4).

Finally several other weak frequencies are detected in the full dataset (1998+1999+2001), but the power is too low for the phase to be accurate, so we do not consider them further.

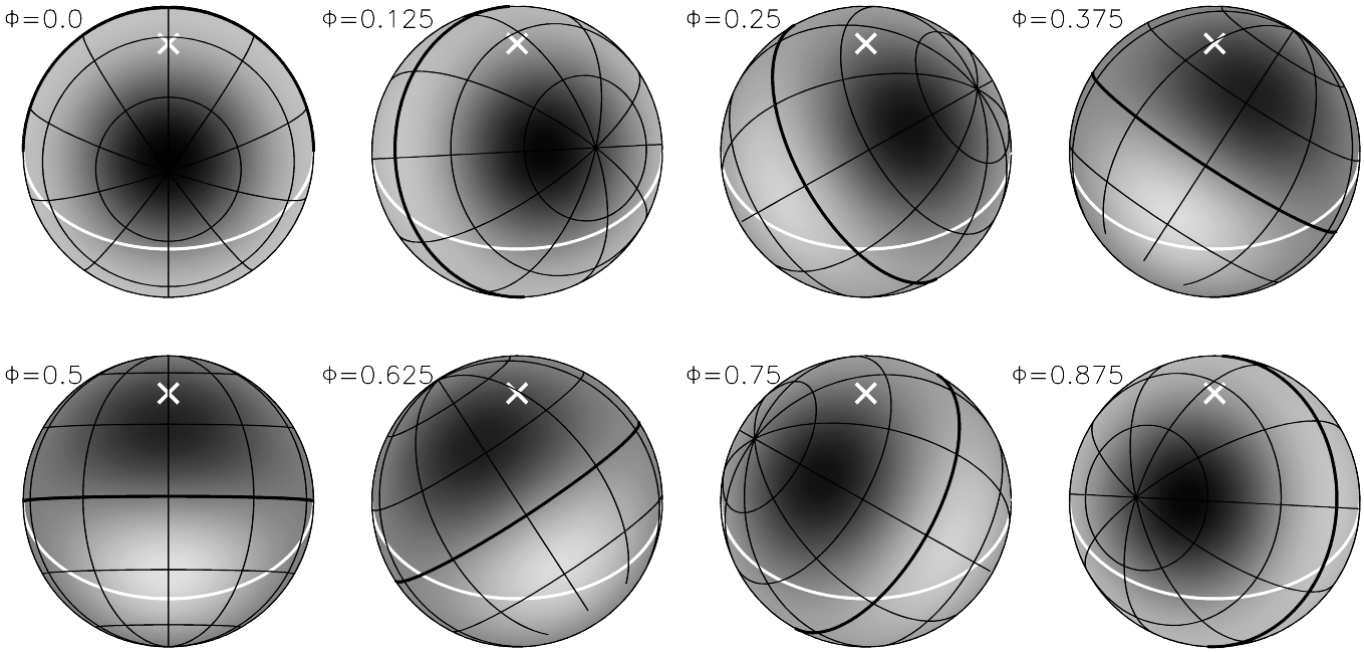

Fig. 12. Greyscale representation of the relative contribution of the magnetic dipole to the integrated longitudinal magnetic field on the visible hemisphere of ω Ori, at different rotational phases with step of $\delta\Phi = 0.125$. The black color corresponds to positive field values and the white color to negative field values. The phase runs from the top left panel to the lower right panel and corresponds to the convention used in Fig. 11. A grid of magnetic longitudes and latitudes is overplotted, with the magnetic equator shown as a thicker black line. The rotation axis and equator are shown with a white cross and line respectively. Although the strongest magnetic field is at the magnetic poles, the positions on the stellar surface that contribute the most to the longitudinal field are not at the poles, due to a geometrical effect and to the limb darkening effect.

8.2. Outbursts

An outburst occured in ω Ori during the MuSiCoS campaign in 1998. It is associated with a cloud of material orbiting around the star with a frequency of 0.46 c d^{-1}, which disappeared after a few revolutions around the star (see N02).

We searched for an outburst in the data collected in 1999 and 2001. No indication of an outburst appeared in 1999 and we consider that ω Ori was in a quiet phase at that time. These observations were indeed obtained very close to the minimum of emission intensity observed in ω Ori by Buil (2001) at the beginning of 2000. In the data obtained in 2001, we see possible indications for the beginning of an outburst in the $V + R$ and V/R variations, but the suggested outburst itself probably occured after the observing run.

8.3. Magnetic field

Despite of the large error bars of the magnetic measurements, we have found evidence for the presence of a magnetic field in the classical Be star ω Ori.

The longitudinal magnetic field varies periodically. The period derived from the magnetic measurements, $P = 1.29$ d, corresponds to the rotational period of the star. The EW of the UV resonance lines also varies periodically. The derived period $P = 1.29$ d is again the rotational period.

The fact that the EW of the UV lines and the longitudinal magnetic field vary with the rotational period is coherent with a magnetic oblique rotator model. The correspondence in phase between the maximum of emission in the UV lines and the maximum magnetic field value cannot be established due to the low accuracy in the determination of the rotation period. However, our model of a magnetic rotating dipole, applied with the parameters of ω Ori, shows that only one of the magnetic pole (the positive pole) passes through the visible hemisphere whereas the other magnetic (negative) pole is always hidden. The same conclusion is reached from the UV measurements which show only one maximum in the EW instead of the two maxima usually observed for a magnetic star for which the two magnetic poles are visible (e.g. ζ Cas, Neiner et al. 2003a). The magnetic results and the UV results are therefore fully compatible.

From our oblique dipole model we derive that the polar magnetic field is $B_{\rm pol} = 530^{760}_{300}$ G. This value is higher than the lower limit of about 300 G obtained by Cassinelli et al. (2002) needed to form a magnetically torqued disk in a rapidly rotating B2 star with its magnetic axis aligned with its rotation axis.

Moreover, the star is found to be N-enriched. This is also the case of β Cep, the only magnetic (low velocity) Be star known up to now (Henrichs et al. 2000), and of ζ Cas, the only magnetic SPB star known up to now (Neiner et al. 2003a). Chemical peculiarities are often found in magnetic stars, because the magnetic field inhibits mixing motions in the outer layers of the star.

8.4. Rotational modulation

A frequency of about $f = 0.77$ c d^{-1} is detected, mainly in the V/R ratio of red He I lines (Fig. 6), but also in other

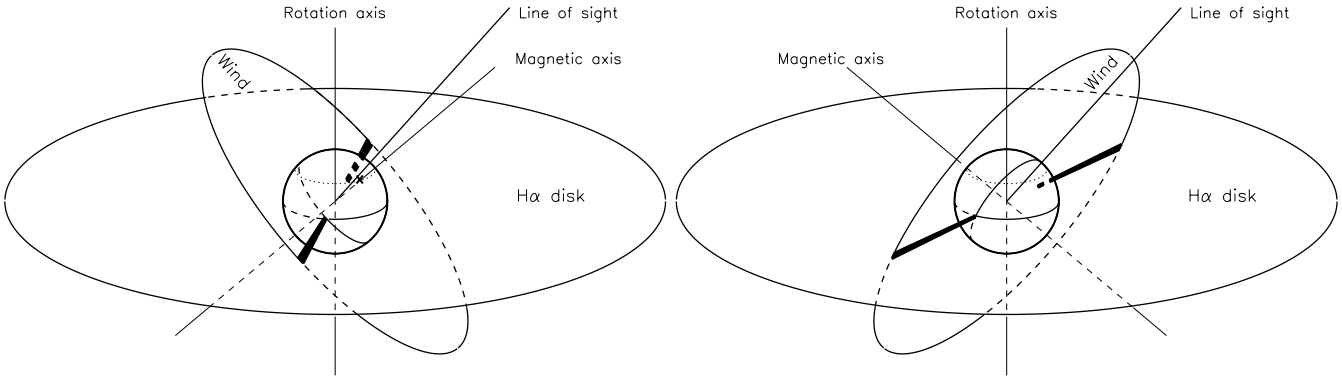

Fig. 13. Sketch of ω Ori. The wind flows from the magnetic poles to the magnetic equatorial plane, while the Hα disk is in the rotation equatorial plane. The intersection regions of the two equators (EIR) are shown. The right- and left hand panels show the same geometrical configuration but half a rotation period apart. The dotted parallel on the stellar surface indicates the position of the magnetic axis as the star rotates. The positive pole is indicated with a cross when it is facing the observer.

observables such as the peak separation of lines with an emission component (Fig. 5) and the minimum line intensities (Fig. 2). This frequency is associated with the rotation period of the star (P = 1.29 d). It is detected with a strong power in the 1999 data and with a lower power in 1998 and 2001. Nevertheless, the V/R ratio of the Hα and Hβ lines observed in 2001 show a clear variation with this frequency (Fig. 7).

From the search for periodicities in the lpv, we find that the V/R ratio of lines with an emission component varies with the rotation period and shows two maxima during one period (Fig. 6). This suggests the presence of two opposite regions of enhanced density corotating with the star. Note that this short-term variations in the V/R ratio is not related to the long-term V/R variations usually associated with one armed oscillations of Be stars disks.

A recent study by Preuss et al. (2003) analyses the regions of equilibrium around a rotating star hosting a magnetic dipole field. They obtain that the regions of stability depend on the angle β between the rotation axis and the magnetic axis. When β is small ($\beta \leq 40°$), the region of equilibrium is the magnetic equator. When β increases ($40° \leq \beta < 90°$), equilibrium is reached in the magnetic equator but also in two regions above the magnetic poles. The size of these polar regions increases with β. Finally at $\beta = 90°$, the regions of stability are the magnetic equator (except a part which contains the rotation axis) and two cones above the magnetic poles.

In our dipole model of ω Ori, $\beta \sim 50°$. According to Preuss et al. (2003) this means that the material ejected from the star, if it is magnetically confined, can end up in a disk in the magnetic equator and/or in two clouds above the magnetic poles. From the geometrical configuration of ω Ori, only the positive magnetic pole is clearly seen, the negative one just appears at the edge of the visible hemisphere. Therefore if the calculation of Preuss et al. applies to ω Ori and the material is in clouds above the poles we would observe only one maximum in the V/R variations at the phase of maximum field. However, we observe two equal maxima in the V/R variations with a phase difference of 0.5. This means that, for ω Ori, the observed clouds are not situated above the magnetic poles.

Let us consider the global picture of a Be star hosting a magnetic dipole. This sketch is shown in Fig. 13 for ω Ori. The usual Hα disk is assumed to be situated in the rotational equatorial plane. The magnetic dipole is oblique, thus its magnetic equator lies in a different plane than the rotational equator. These two planes intersect in two regions, opposite to each other, hereafter refered as the Equators Intersection Regions (EIR). If the magnetic field is weak, magnetic confinement can only occur close to the star and thus the EIR are close to the stellar surface. Note that the EIR corotate with the rotation period. In Fig. 12, the EIR are situated at the intersections of the thick white and black lines.

The wind material, flowing from the magnetic poles along the field lines, is led to the magnetic equator. As the star rotates, the magnetic equator plane corotates and is dragged through the rotational equator. If the magnetic field is strong enough compared to the rotation velocity, the material is strongly confined in the magnetic equator and the disk is formed there. This is the case for the star β Cep (Henrichs et al. 2000; Donati et al. 2001), which hosts a weak magnetic field (about 300 G) and is a very slow rotator (v = 28 km s^{-1}). On the contrary, if the rotation velocity of the star is high enough compared to the strength of the magnetic field (e.g. for classical Be stars), the material tends to go into the rotational equator and forms a disk there. Two cases can be considered: either the wind material, following the field lines, first meets the rotational equator and stays there, conserving its angular momentum instead of following the field lines further to the magnetic equator, or it first meets the magnetic equator and then flows to the rotational equator via the EIR. In both cases, the material ends up in the rotational equator plane.

As all the involved forces contribute to put material in the EIR, it is probable that they are denser than the rest of the disk where the magnetic and rotation forces diverge, i.e. there are clouds at the EIR positions. We then expect to see emission from the intersection regions and a V/R variation similar to the one observed in the Hα and Hβ lines of ω Ori in 2001 (Fig. 7), i.e. two slow decreases of the V/R ratio, each of them followed by a sudden increase at the phase of maximum and minimum field. This corresponds to the phases 0 and 0.5 in Fig. 12, when the two clouds (intersections of the thick white and black lines)

are on the side of the star. The variation in the peak separation of Hβ in 2001 (Fig. 5) may then be explained as a projection effect of the magnetic equator, and thus of the clouds, on the stellar visible hemisphere as the star rotates. The magnetic equator and clouds are seen face on and from the side at the phases 0 and 0.5 respectively.

However, the contrast in density, between the clouds and the disk, is probably stronger at epochs when the whole disk density is lower, i.e. close to the minimum emission phase of the star. At epochs where the disk is filled up by strong ejections of material, the EIR clouds are probably hard to detect. That would explain why the rotation frequency and the clouds are better detected in the observations obtained in 1999 and 2001 than in the data of 1998 for example and why it has not been detected in earlier observations when ω Ori was in a phase of stronger emission.

8.5. Comparison with σ Ori E

In Bp stars, such as the He-strong star σ Ori E, patches of specific chemical abundances have been observed on the stellar surface, in particular patches of enhanced helium abundance at the wind base, due to chemical fractionation, i.e. decoupling of the helium from the metals in the stellar wind (Groote & Hunger 1997). This has not been observed in ω Ori, which is not a Bp star.

However, the magnetic star σ Ori E also shows clouds of material attached to the photosphere, at the intersection regions of the rotational and magnetic equatorial planes (Short & Bolton 1994). As this star does not host a disk, the clouds are detected more easily. We propose that the equatorial clouds of σ Ori E and ω Ori build up in the same way.

Acknowledgements. We are grateful to C. Aerts and L. Balona for providing the data they obtained in 1999. We thank the referee, T. Rivinius, for constructive discussions. Y.F. is supported by a Marie Curie Individual Fellowship of the European Community programme FP5 under contract number HPMF-CT-2000-00497. This research has made use of the Simbad database maintained at CDS, Strasbourg, France.

References

Andrievsky, S. M., Korotin, S. A., Luck, R. E., & Kostynchuk, L. Y. 1999, A&A, 350, 598
Balona, L. A., Aerts, C., Božić, H., et al. 2001, MNRAS, 327, 1288 (B01)
Buil, C. 2001, Atlas of Be stars on the web
http://www.astrosurf.com/buil/us/bestar.htm
Cardelli, J. A., Clayton, G. C., & Mathis, J. S. 1989, ApJ, 345, 245
Cassinelli, J. P., Brown, J. C., Maheswaran, M., Miller, N. A., & Telfer, D. C. 2002, ApJ, 578, 951
Chauville, J., Zorec, J., Ballereau, D., et al. 2001, A&A, 378, 861
Claret, A. 2000, A&A, 363, 1081
Collins, G. W., Truax, R. J., & Cranmer, S. R. 1991, ApJS, 77, 541
Dimitrijevic, M. S., Djenize, S., Sreckovic, A., & Bukvic, S. 2002, in IAU Symp. 210, Modelling of Stellar Atmospheres, held in Sweden, June 2002
Donati, J.-F., Semel, M., Carter, B. D., Rees, D. E., & Collier Cameron, A. 1997, MNRAS, 291, 658
Donati, J.-F., Wade, G. A., Babel, J., et al. 2001, MNRAS, 326, 1265
Fabregat, J., & Reglero, V. 1990, MNRAS, 247, 407
Frémat, Y., Levenhagen, R., Zorec, J., et al. 2002, in SF2A-2002, held in Paris, France, June 2002, ed. F. Combes, & D. Barret, (EDP-Sciences)
Frémat, Y., & Zorec, J. 2003, A&A, in preparation
Gies, D. R., & Lambert, D. L. 1992, ApJ, 387, 673
González, V. R., Aparicio, J. A., & del Val, J. A. 2000, A&A, 363, 1177
Grevesse, N., & Sauval, A. J. 1998, Space Sci. Rev., 85, 161
Groote, D., & Hunger, K. 1997, A&A, 319, 250
Gummersbach, C. A., Kaufer, A., Schaefer, D. R., Szeifert, T., & Wolf, B. 1998, A&A, 338, 881
Henrichs, H. F., de Jong, J. A., Donati, J.-F., et al. 2000, in ASP Conf. Ser. 214, The Be Phenomenon in Early-Type Stars, IAU Coll. 175, ed. M. A. Smith, H. F. Henrichs, & J. Fabregat, 324
Henrichs, H. F., Kaper, L., & Nichols, J. S. 1994, A&A, 285, 565
Hubeny, I., & Lanz, T. 1995, ApJ, 439, 875
Lanz, T., Dimitrijevic, M. S., & Artru, M.-C. 1988, A&A, 192, 249
Neiner, C., Geers, V. C., Henrichs, H. F., et al. 2003a, A&A, 406, 1019
Neiner, C., Henrichs, H. F., Floquet, M., et al. 2003b, A&A, in press
Neiner, C., Hubert, A.-M., Floquet, M., et al. 2002, A&A, 388, 899 (N02)
O'Donnell, J. E. 1994, ApJ, 422, 158
Osaki, Y. 1986, PASP, 98, 30
Peters, G. 1996, Be Star Newsletter, 31, 16
Preuss, O., Holzwarth, V., Solanki, S. K., & Schuessler, M. 2003, A&A, submitted
Rivinius, T., Baade, D., Štefl, S., et al. 1998a, A&A, 333, 125
Rivinius, T., Baade, D., Štefl, S., et al. 1998b, in Cyclical Variability in Stellar Winds, 207
Schaller, G., Schaerer, D., Meynet, G., & Maeder, A. 1992, A&AS, 96, 269
Shore, S. N. 1987, AJ, 94, 731
Shore, S. N., & Brown, D. N. 1990, ApJ, 365, 665
Short, C. I., & Bolton, C. T. 1994, Pulsation; Rotation; and Mass Loss in Early-Type Stars, ed. L. A. Balona, H. F. Henrichs, & J. M. Le Contel, in IAU Symp., 162, 171
Sonneborn, G., Grady, C. A., Wu, C., et al. 1988, ApJ, 325, 784
Underhill, A. B. 1987, in Physics of Be Stars, IAU Colloq., 92, 411